

# Slip and friction at fluid-solid interfaces: Concept of adsorption layer

Haodong Zhang,<sup>1,2</sup> Fei Wang,<sup>1,2,\*</sup> and Britta Nestler<sup>1,2,3</sup>

<sup>1</sup>*Institute of Applied Materials-Microstructure Modelling and Simulation,  
Karlsruhe Institute of Technology (KIT),  
Strasse am Forum 7, Karlsruhe 76131, Germany.*

<sup>2</sup>*Institute of Nanotechnology, Karlsruhe Institute of Technology (KIT),  
Hermann-von-Helmholtz-Platz 1, Eggenstein-Leopoldshafen 76344, Germany*

<sup>3</sup>*Institute of Digital Materials Science,  
Karlsruhe University of Applied Sciences,  
Moltkestrasse 30, Karlsruhe 76133, Germany*

(Dated: February 4, 2026)

# Abstract

When a fluid flows past a solid surface, its macroscopic motion arises from a subtle interplay between microscopic hydrodynamic and thermodynamic effects at the fluid–solid interface. Classical hydrodynamic models often rely on an unphysical no-slip boundary condition or an arbitrarily prescribed slip length  $l_s$ , yet both approaches lack a rigorous physical foundation. This work introduces the concept of an Adsorption Layer (AL), an interfacial region of thickness  $\delta l$ , where fluid-solid molecular interactions regulate both surface adsorption/depletion and interfacial slip. By applying the energy minimization principle, we derive balance equations within the AL that couple fluid-solid friction, viscous stresses, and surface adsorption dynamics. This framework establishes a self-consistent thermodynamic coupling between the AL and the bulk fluid, unlike conventional sharp-interface models. A key finding is the often-overlooked role and coupling of pressure and chemical potential gradients in the direction normal to the interface. This theoretical advance successfully explains the confinement-induced enhancement of water slippage in carbon nanotubes, quantitatively agreeing with molecular dynamics and experimental data—an effect classical slip models fail to reproduce. Furthermore, when extended to binary liquids, the theory captures spatial variations in slip velocity near moving contact lines, highlighting the role of interfacial friction in shaping local flow. Our results demonstrate that the slip length is not a fixed material constant but rather an emergent, geometry- and composition-dependent property arising from coupled interfacial thermodynamics and hydrodynamics. This framework provides a physically grounded description of interfacial momentum transfer, with significant implications for microfluidics and surface engineering.

## I. INTRODUCTION

When a moving fluid interacts with a solid substrate, the velocity field near the surface forms a boundary layer, which can be broadly categorized into the following classical regimes.

(I) *No-Slip Boundary Condition*: From a macroscopic viewpoint, extensive experimental and theoretical investigations [32, 35, 59] support the no-slip condition  $\mathbf{u}_s = \mathbf{0}$ , implying zero fluid velocity at the fluid–solid interface S, as illustrated in figure 1(I). This condition

---

\* fei.wang@kit.edu

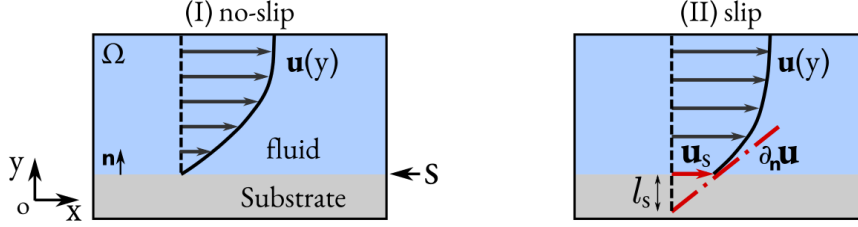


FIG. 1. (I) Fluid velocity distribution  $\mathbf{u}(y)$  with no-slip boundary condition at fluid-substrate contacting surface  $S$ . (II) Slip boundary condition enables non-zero fluid velocity  $\mathbf{u}_s$  at  $S$ . The Navier slip length is mathematically defined as  $l_s = \mathbf{u}_s / \partial_n \mathbf{u}$ .

has long been regarded as a cornerstone of continuum fluid mechanics. With the emergence of computational fluid dynamics, it became a standard modeling assumption due to its strong predictive accuracy in a wide range of flow problems [17, 43, 63, 64]. However, this assumption introduces several conceptual inconsistencies. First, the solid–fluid boundary under the no-slip condition does not dissipate mechanical energy. Taking laminar Poiseuille flow as an example, the total energy dissipation rate can be expressed as

$$\frac{d\mathcal{L}}{dt} = - \int_{\Omega} \eta \nabla \mathbf{u} : \nabla \mathbf{u} d\Omega \leq 0,$$

indicating the energy is dissipated solely within the bulk fluid domain  $\Omega$  through viscous stresses governed by the dynamic viscosity  $\eta$  and the velocity gradient  $\nabla \mathbf{u}$ . Second, numerous nanoscale experiments have revealed measurable slip velocity at the fluid–solid interface [36, 40, 42, 61], a finding further corroborated by molecular dynamics (MD) simulations [1, 30, 44, 46, 47, 54]. These results challenge the universality of the no-slip condition and underscore the need for refined boundary models.

*(II) Navier Slip Boundary Condition (NBC):* This concept of interfacial slip dates back to the seminal works of [37, 41]. Here slip is characterized by the slip length  $l_s$  [31, 33, 62], defined by

$$\mathbf{u}_s = l_s \partial_n \mathbf{u}, \quad (1)$$

where  $\partial_n \mathbf{u}$  denotes the velocity gradient normal to the solid substrate; see figure 1(II). Experimental observations show that  $l_s$  can vary from nanometers to micrometers [27, 39], depending on interfacial properties and topography. In confined geometries, such as carbon nanotubes, reported slip lengths can be several orders of magnitude larger than those

observed in macroscopic systems [50]. Under the slip boundary condition, the total energy dissipation rate becomes

$$\frac{d\mathcal{L}}{dt} = - \int_S (\eta/l_s) \mathbf{u}_s^2 dS - \int_\Omega \eta \nabla \mathbf{u} : \nabla \mathbf{u} d\Omega \leq 0. \quad (2)$$

Here, both bulk and interfacial dissipation contribute to the overall energy loss. As  $l_s$  increases, interfacial dissipation weakens accordingly. In practice, the slip length  $l_s$  is not known *a priori* and must be determined indirectly—through flow-rate measurement, interfacial force experiment, or MD simulation. To connect interfacial friction to hydrodynamic quantities,  $l_s$  is often related to the intrinsic friction coefficient  $\lambda_{\text{intr}}$  via

$$l_s = \frac{\eta}{\lambda_{\text{intr}}}. \quad (3)$$

Accordingly, the first term in (2) represents the dissipation by the interfacial friction force,

$$\mathbf{F} = -\lambda_{\text{intr}} \mathbf{u}_s,$$

where  $\lambda$  can be evaluated from equilibrium MD simulations using the Green–Kubo relation [4],

$$\lambda_{\text{intr}} = \frac{1}{Sk_B T} \int_0^\infty dt \langle \mathbf{F}(\mathbf{x}, t), \mathbf{F}(\mathbf{x}, 0) \rangle, \quad (4)$$

in which  $k_B$  and  $T$  denote the Boltzmann constant and temperature, respectively. This method has been successfully applied to quantify slippage in diverse interfacial systems, from hydrophobic surfaces to carbon nanotubes [14, 50]. Nonetheless, the computational cost of MD simulations shows their applicability only to nanoscale or submicron systems; they also remain impractical for multicomponent flows at larger scales. With the friction coefficient, NBC (1) is also expressed as

$$\lambda_{\text{intr}} \mathbf{u}_s = \eta \nabla \mathbf{u} \cdot \mathbf{n}.$$

(III) *Generalized Navier boundary condition (GNBC)*: A complementary mean-field perspective treats the fluid–solid interface as a sharp boundary where intermolecular interactions induce depletion/adsorption layers [15, 57, 70], thereby modulating wetting and dewetting dynamics at the macroscopic level. During the wetting induced flow, these interactions also generate hydrodynamic damping near the wall, producing velocity gradients consistent with interfacial slip [22, 60].

Building on molecular insights, [44] derived GNBC for a two-dimensional coordinate system  $(x, n)$ , relating the slip velocity  $\mathbf{u}_s = (u_s, v_s)$  to fluid-solid interfacial force balance as,

$$\lambda_{\text{intr}} \mathbf{u}_s = -\eta (\partial_n \mathbf{u}_s + \partial_x v_s) + \tilde{\mu}_s \partial_x c_s, \quad (5)$$

where the non-uniform surface composition  $c_s$  leads to an extra capillary term into NBC. Here, the surface chemical potential of sharp interface model is defined as  $\tilde{\mu}_s = \kappa \nabla c_s \cdot \mathbf{n} + \partial \gamma / \partial c_s$  with  $\gamma$  denoting the fluid-solid interfacial tension. The surface composition then evolves by the dynamic wetting boundary condition, following the mean curvature flow as

$$\frac{\partial c_s}{\partial t} = -\tau \tilde{\mu}_s, \quad (6)$$

where the kinetic parameter  $\tau$  controls the surface diffusion. Including the composition diffusive dissipation, the total energy dissipation rate becomes,

$$\frac{d\mathcal{L}}{dt} = - \int_S \lambda_{\text{intr}} u_s^2 dS - \int_S \tau \tilde{\mu}_s^2 dS - \int_\Omega \eta \nabla \mathbf{u} : \nabla \mathbf{u} d\Omega - \int_\Omega M (\nabla \mu)^2 d\Omega \leq 0.$$

The GNBC model has been validated against MD simulations of binary Couette flows, showing quantitative agreement. Nevertheless, a key limitation of Qian's formulation is that interfacial energy dissipation is established under steady force balance conditions, implying that (5) represents a steady-state slip law rather than a fully dynamic one.

(IV) *Dynamic slip boundary condition*: The slippage under non-equilibrium condition was first systematically analyzed in the seminal work of [3]. By evaluating the total surface energy dissipation at the fluid–solid dividing surface, he derived the interfacial momentum balance as,

$$\rho_s \frac{d\mathbf{u}_s}{dt} = \nabla_s \cdot [\gamma (\mathbf{I} - \mathbf{n} \otimes \mathbf{n}) + \eta (\nabla_s \mathbf{u}_s + \nabla_s \mathbf{u}_s^T)] + \mathbf{F}. \quad (7)$$

where  $\gamma$  denotes the surface tension and  $\mathbf{F}$  represents the net external force acting along the interface. The surface gradient operator is defined as  $\nabla_s := \nabla - \mathbf{n}(\mathbf{n} \cdot \nabla)$ . Here, the surface density follows the material conservation law [3],

$$\partial \rho_s / \partial t + \nabla_s \cdot (\rho_s \mathbf{u}_s) = 0, \quad (8)$$

which is more rigorous than the non-conserved (6). Using the entropy production principle, [6] subsequently obtained the same result from the second law of thermodynamics,

employing a linear closure approach to formulate a more generalized interfacial velocity boundary condition (see also [5] for detailed derivations). At the steady state  $\partial \mathbf{u}_s / \partial t = 0$  and neglecting the inertia term  $\mathbf{u}_s \cdot \nabla \mathbf{u}_s$ , the momentum balance (7) reduces to GNBC (5).

In these foundational works [3, 6, 44], the emphasis lies primarily on deriving the governing interfacial equations. Determining the actual slippage at the fluid–solid interface, however, often requires numerical simulations.

To complement simulation-based approaches, earlier analytical efforts focused on the slip at fluid–solid interface always adopt either of the above four formulations. In the seminal wedge flow model by [25, 38], analytical solutions for the local flow field of the liquid–air–solid system near the contact line is obtained under the no-slip boundary condition. However, this formulation produces a shear-stress singularity at the contact line.

To resolve this issue, [23] incorporated the NBC at the liquid–solid interface, obtaining a finite frictional force associated with the motion of the fluid along the solid substrate. Based on this framework, subsequent studies [12, 29, 52] developed the generalized lubrication theory, extending Hocking’s results to the slippage of both Newtonian and viscoelastic fluids.

In addition, all these analytical models treat the fluid as a compositionally homogeneous medium, neglecting interfacial variations in density or concentration. To incorporate surface depletion/adsorption effects into the wedge-flow framework, [51] proposed the interface formation model, which corresponds to the steady state of dynamic slip boundary condition to include surface density variations. The steady state of (7) is expressed in two-dimensional case with  $\mathbf{u}_s = (u_s, 0)$  as,

$$\lambda_{\text{intr}} u_s = \nabla_s [\gamma_0 (\rho_s - \rho_e)] - \nabla_s \cdot [\eta (\nabla_s u_s + \nabla_s u_s^T)], \quad (9)$$

where the slippage results in surface density  $\rho_s$  deviating from the equilibrium  $\rho_e$ , and generates capillary pressure scaled by the surface tension parameter  $\gamma_0$ . The surface density further evolves according to the surface density boundary condition,

$$\partial \rho_s / \partial t + \nabla_s \cdot (\rho_s u_s) = -\Gamma (\rho_s - \rho_e), \quad (10)$$

where  $\Gamma$  is the surface-tension relaxation parameter and related with the kinetic parameter  $\tau$  in (6) of GNBC. (10) bears strong analogy to the dynamic wetting boundary condition (6), which is absent from generalized lubrication model. But, the formulation for surface density

is expressed in a non-conserved form which is not compatible with the thermodynamic framework with the material conservation law (8).

In the present study, we develop a thermodynamically consistent formulation of dynamic surface slip for multicomponent fluids, incorporating both slip and wetting boundary conditions within a sharp-interface framework. Our framework integrates thermodynamic consistency—following the sharp-interface and phase-field formalism [57, 65]—with hydrodynamic theory grounded in interfacial momentum conservation [21, 48]. This combination enables a unified description of slip phenomena that captures both thermodynamic and hydrodynamic contributions at the fluid–solid interface.

A central distinction from previous slip models lies in the treatment of pressure at the fluid–solid interface. Classical models with the incompressible assumption treat pressure as an auxiliary field introduced solely to enforce the constraint  $\nabla \cdot \mathbf{u} = 0$ , and therefore omit it entirely from the slip boundary condition. In contrast, our adsorption-layer (AL) formulation assigns physical volume to the interfacial molecules, endowing them with a well-defined pressure that must remain thermodynamically coupled to the bulk. This coupling becomes especially important in flows driven by pressure gradients—such as Poiseuille flow—where the interfacial pressure must respond to the bulk pressure gradient rather than being artificially excluded. Incorporating this pressure coupling enables our model to reproduce the confinement-enhanced water slippage observed in carbon nanotubes, an effect that cannot be explained by existing sharp-interface slip models

The remainder of this paper is organized as follows. Section 2 introduces the total energy functional and derives the dynamic wetting-slip boundary condition governing interfacial dynamics through the energy minimization principle. The distinctions between our model and previous theories are clarified. Section 3 presents the validation of our model and examines flow behaviors influenced by the proposed wetting–slip boundary condition, including classical configurations such as Poiseuille and Couette, and wedge flows.

## II. MODEL DESCRIPTION

The governing equations for material and momentum evolution in the bulk fluid are not the primary focus of this study; they follow the standard Cahn–Hilliard–Navier–Stokes (CHNS) formulation and are not reproduced here (see Appendix A 6 and [68] for detailed

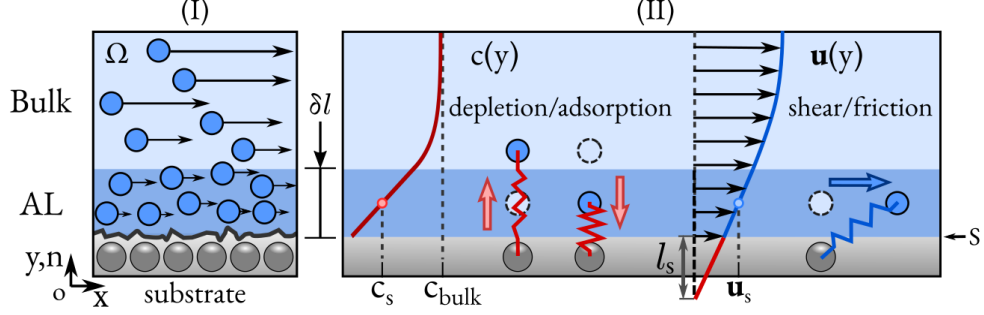


FIG. 2. (I) Illustration of fluid passing the solid substrate. Solid-fluid molecular interactions form the adsorption layer (AL) above the solid surface  $S$ . (II) Solid-fluid molecular interactions perpendicular to  $S$  leads to surface depletion/adsorption which modifies surface composition  $c_s$  deviating from the bulk fluid. Interactions parallel to  $S$ , such as bond rotation, results in shear/friction which changes the velocity profile  $\mathbf{u}$ .

derivation).

In contrast, the present work concentrates on the fluid–solid contact region, where molecular interactions play a dominant role. Rather than treating this interface as a mathematically sharp boundary of zero thickness, we adopt the concept of adsorption layer (AL), analogous to the Helmholtz layer in electrical double-layer (EDL) theory. In this framework, the fluid–solid interface is modeled as a thin layer of finite physical thickness  $\delta l$ , within which the fluid–solid molecular interactions are significant; see figure 2(I).

## A. Total energy functional at fluid-solid interface

### 1. Chemical Free Energy

Within this interfacial layer, denoted as the adsorption layer (AL), the local free energy density comprises contributions from mixture entropy, mixture enthalpy, and van der Waals interactions [16, 56]. Accordingly, the interfacial free energy density is expressed as,

$$f_w(c) = h_w(c) - T s_w(c) + f_{vdW}.$$

where  $h_w$  and  $s_w$  are the local enthalpy and entropy densities of the fluid mixture in AL. The absolute temperature is  $T$ , and  $f_{vdW}$  represents the contribution of van der Waals interactions between solid and fluid molecules. The latter modifies the effective poten-

tial energy landscape of the fluid near the solid substrate and can be evaluated using a Lennard–Jones–type potential energy density. Because  $f_w$  depends on the local composition  $c(\mathbf{x})$ , the interfacial free energy naturally becomes composition-dependent. Given that AL is typically much thinner than the bulk region, we define an average surface composition, similar to the average ion concentration in the EDL of Helmholtz model as

$$c_s = \frac{1}{\delta l} \int_0^{\delta l} c(\mathbf{x}) d\mathbf{x}.$$

The interfacial free energy density  $f_w$  can be locally expanded about the average surface composition  $c_s$ , to obtain a Cahn–Hilliard-type formulation, following the methodology developed in our previous work [10]. Consequently, the total chemical free energy functional of the fluid–solid interface is written as

$$\mathcal{F}_s = \int_S dS \int_0^{\delta l} f_w(c(\mathbf{x})) d\mathbf{x} = \int_S \left[ f_w(c_s) + \frac{\kappa_s}{2} (\nabla c_s)^2 \right] \delta l dS$$

where the integration is performed over the macroscopic interfacial area  $S$ . In this expansion, the term proportional to the surface composition gradient accounts for the excess energy arising from compositional inhomogeneity along the interface. Here,  $\kappa_s$  is the surface gradient energy coefficient, quantifying the excess free energy associated with local composition variations along the interface.

As illustrated schematically in figure 2(II), within the thin layer of thickness  $\delta l$  immediately above the uppermost layer of solid molecules, fluid molecules experience depletion/adsorption forces arising from fluid–solid molecular interactions. These forces induce a gradual decay (or enrichment) of the local composition from the AL towards the bulk fluid region, as depicted by the red solid line in figure 2(II).

## 2. Kinetic Energy

In addition to the chemical free energy, the fluid within the adsorption layer also carries kinetic energy, which is characterized by the height-averaged slip velocity, namely,

$$\mathbf{u}_s = \frac{1}{\delta l} \int_0^{\delta l} \mathbf{u}(\mathbf{x}) d\mathbf{x},$$

representing the averaged tangential motion of fluid molecules within the AL [24]. Consequently, the total kinetic energy contained in AL is expressed as

$$\mathcal{K}_s = \frac{1}{2} \int_S dS \int_0^{\delta l} \int_0^{\delta l} d\mathbf{x} d\mathbf{x}' \langle \rho \mathbf{u}(\mathbf{x}), \mathbf{u}(\mathbf{x}') \rangle = \int_S \frac{\rho \mathbf{u}_s^2}{2} \delta l dS,$$

where  $\rho$  denotes the local fluid density. The representative slip velocity  $\mathbf{u}_s$  is defined at the barycentric plane of the adsorption layer (i.e., at  $y = \delta l/2$ ), consistent with experimental observations of polymeric wall slip [13]. This positioning reflects the physical locus at which the tangential momentum transfer between the fluid and solid is most effectively mediated.

### 3. Potential Energy

For fluid systems, there is also the potential energy stored within the adsorption layer as

$$\mathcal{P}_s = \int_S dS \int_0^{\delta l} p(\mathbf{x}) d\mathbf{x} = \int_S p_s \delta l dS,$$

where  $p_s$  denotes the average potential energy density in AL.

## B. Energy minimization principle

Following the thermodynamic framework of [3, 6, 44, 68], the governing equations within the adsorption layer can be systematically derived from the energy minimization principle. Detailed deductions are documented in the Appendix A 7. The resulting dissipation contains two concurrent minimizing mechanisms that govern interfacial dynamics.

### 1. Energy Dissipation via Surface Diffusion

The first mechanism corresponds to surface diffusion, which governs interfacial material transport and manifests itself through the wetting boundary condition:

$$\frac{\partial c_s}{\partial t} + \mathbf{u}_s \cdot \nabla c_s = \nabla \cdot (M_s \nabla \mu_s), \quad (11)$$

where  $M_s$  is the surface diffusion mobility and  $\mu_s := \partial f_w / \partial c_s - \kappa_s \nabla^2 c_s$  is the surface chemical potential defined in the adsorption layer [19].

Here, (11) takes the Cahn–Hilliard form, reflecting the conserved nature of material transport within the physically finite AL. In contrast, earlier sharp-interface formulations [44, 65], treated the interface as a mathematically infinitesimal (“ghost”) layer governed by a non-conserved Allen–Cahn type formulation, such as (6). Our model treats the AL as a genuine interfacial region with finite volume, consistent with the Helmholtz-layer analogy in

the EDL. Material conservation within this layer becomes essential when modeling charge or ion transport, motivating our use of the conserved form. As shown in Appendix B1, the Allen–Cahn and Cahn–Hilliard forms become mathematically equivalent under specific limits, ensuring formal consistency with previous models while reinstating their physical interpretation.

Our wetting boundary condition (11) is structurally analogous to the surface density conservation equation (8), assuming a linear relation between surface density  $\rho_s$  and composition  $c_s$ . Two distinctions, however, should be emphasized. First, the convective term in our formulation appears as  $\mathbf{u}_s \cdot \nabla c_s$ , rather than  $\nabla \cdot (\rho_s \mathbf{u}_s)$  in their treatment. The two expressions are equivalent under the incompressibility constraint  $\nabla \cdot \mathbf{u}_s = 0$ , ensuring full consistency with continuum mechanics. Second, we incorporate composition-driven surface diffusion, which becomes significant in heterogeneous interfacial systems.

## 2. Energy Dissipation via Convection

The second dissipation channel arises from momentum convection associated with interfacial slippage. Averaging the momentum over the adsorption layer yields [24]:

$$\frac{d(\rho \mathbf{u}_s)}{dt} \delta l = \nabla \cdot \underline{\underline{\mathbf{T}}_s} \delta l + \mathbf{F}. \quad (12)$$

where the stress tensor in AL reads

$$\underline{\underline{\mathbf{T}}_s} = -p_s \mathbf{I} + \kappa_s \nabla c_s \otimes \nabla c_s + \eta (\nabla \mathbf{u}_s + \nabla \mathbf{u}_s^T).$$

The last term on the right-hand side (*rhs*) of (12) corresponds to the Stokes-type drag arising from all external forces. In this study,  $\mathbf{F}$  is identified as the fluid–solid friction, which plays a central role in controlling interfacial momentum transfer and slip.

To explicitly determine the form of  $\mathbf{F}$ , we consider the microscopic origin of friction within AL. As illustrated in figure 2(II), molecular slippage within the adsorption layer (AL) induces local bond rotation and elongation between the substrate and adjacent fluid molecules. Following the hydrodynamic model of [4], the rate of energy dissipation due to fluid–solid friction—under a linear response approximation—can be expressed as

$$dE_s/dt = - \int_0^{\delta l} \int_0^{\delta l} d\mathbf{x} d\mathbf{x}' \langle \lambda(c(\mathbf{x})) \mathbf{u}(\mathbf{x}), \mathbf{u}(\mathbf{x}') \rangle = -\lambda(c_s) \mathbf{u}_s^2 \delta l,$$

so that the height-averaged friction coefficient  $\lambda(c_s)$  also depends on the local surface composition  $c_s$ . The mean frictional force acting on the fluid within the AL is thus

$$\mathbf{F} = (dE_s/dt)/\mathbf{u}_s = -\lambda(c_s) \mathbf{u}_s \delta l.$$

Unlike sharp-interface models where  $\delta l \rightarrow 0$ , our finite-thickness formulation explicitly introduces  $\delta l$  as a characteristic momentum-dissipation scale, thereby linking slip attenuation directly to the range of solid–fluid molecular interactions.

Moreover, (12) is also expressed as

$$\frac{d(\rho \mathbf{u}_s)}{dt} = -\nabla P_s - c_s \nabla \mu_s + \nabla \cdot [\eta(\nabla \mathbf{u}_s + \nabla \mathbf{u}_s^T)] - \lambda \mathbf{u}_s, \quad (13)$$

where the grand pressure is defined as  $P_s = p_s + f_w + \kappa_s(\nabla c_s)^2 - \mu_s c_s$ . The detailed deduction is documented in the Appendix A 7.

### 3. Thermodynamic Consistency and Isothermal Approximation

While the above derivation follows an energy-minimization route, it remains fully consistent with the entropy principle of [3, 5]. Those studies naturally incorporate interfacial heat and entropy fluxes for non-isothermal systems, whereas our present model focuses on the isothermal limit. In the following part, we will discuss the connection of both approaches and their thermodynamically equivalence under specified conditions.

As deduced in Appendix A 8, the total energy dissipation rate at the fluid–solid interface under isothermal condition is

$$\frac{d\mathcal{L}_s(c_s, \mathbf{u}_s; T)}{dt} = \frac{d(\mathcal{F}_s + \mathcal{K}_s + \mathcal{P}_s)}{dt} = -\int_S [M_s(\nabla \mu_s)^2 + \eta \nabla \mathbf{u}_s : \nabla \mathbf{u}_s + \lambda \mathbf{u}_s^2] \delta l dS \leq 0.$$

Including the entropy  $\mathcal{S}$  related to the thermal effects recovers total energy conservation

$$\mathcal{L}_s(c_s, \mathbf{u}_s, T) + T\mathcal{S} = \text{constant},$$

and the entropy production rate becomes

$$\frac{d\mathcal{S}}{dt} = -\frac{1}{T} \frac{d\mathcal{L}_s(c_s, \mathbf{u}_s, T)}{dt} = -\frac{1}{T} \frac{d\mathcal{L}_s(c_s, \mathbf{u}_s; T)}{dt} - \frac{1}{T} \frac{\partial \mathcal{L}_s}{\partial T} \frac{dT}{dt},$$

where  $\partial \mathcal{L}_s / \partial T$  defines the thermo-chemical potential. By introducing thermal conductivity  $K$ , we recover Fourier’s heat equation:

$$dT/dt = \nabla \cdot [K \nabla (\partial \mathcal{L}_s / \partial T)] = \nabla \cdot (\kappa_T \nabla T),$$

with the thermal diffusivity  $\kappa_T = K\partial^2\mathcal{L}_s/\partial T^2$ . Hence, the total entropy production rate is

$$\frac{d\mathcal{S}}{dt} = \frac{1}{T} \int_S [\kappa_T(\nabla T)^2 + M_s(\nabla\mu_s)^2 + \eta\nabla\mathbf{u}_s : \nabla\mathbf{u}_s + \lambda\mathbf{u}_s^2] \delta l \, dS \geq 0,$$

This means when temperature evolution is considered, our energy minimization formulation is strictly equivalent to the entropy maximization principle of [3, 5].

For typical liquids, such as water under moderate slip velocities, the interfacial heating generated by friction is minimal, and the isothermal approximation remains valid. Using the molecular dynamics estimation [7] with  $\lambda \sim 10^{14}\text{kg}/(\text{m}^3\text{s})$  for water confined in carbon nanotube, the effective Prandtl number can be estimated as

$$\text{Pr} = \frac{\text{Momentum diffusivity by friction force}}{\text{Thermal diffusivity}} = \frac{\lambda\delta l^2/\rho}{\kappa_T/(c_p\rho)} \approx 7.6 \text{ (for water)},$$

indicating that momentum diffusion due to friction dominates over thermal diffusion. Thus, for short-time interfacial processes at ambient conditions, the isothermal energy-minimizing framework employed here is an accurate and physically justified approximation.

### III. RESULTS AND DISCUSSION

Based on the evolution equations within the adsorption layer, (11) characterizes the dissipation of chemical free energy driven by surface diffusion, while (12) governs the dissipation of kinetic energy associated with interfacial slippage. Both processes are intrinsically coupled through the slip velocity  $\mathbf{u}_s$ .

Regarding the momentum equation in the AL, (12) now serves as a dynamic momentum evolution equation describing the development and dissipation of the slip velocity under the combined influence of viscous, capillary, and frictional stresses. From a computational perspective, this modification can be readily incorporated into existing Navier–Stokes solvers by embedding AL as a thin interfacial region, where the friction term is explicitly introduced without needs for major structural alterations to the solver.

Our AL-based momentum equation can also recover the generalized Navier boundary condition (GNBC), when the following four assumptions are satisfied: (i) at steady-state condition  $\partial\mathbf{u}_s/\partial t = 0$  and (ii) negligible fluid inertia  $\rho\mathbf{u}_s \cdot \nabla\mathbf{u}_s = 0$ , (12) reduces to the local force balance:

$$\lambda\mathbf{u}_s\delta l = \eta(\nabla\mathbf{u} + \nabla\mathbf{u}^T) \cdot \mathbf{n} + [-\nabla P_s - c_s\nabla\mu_s + \nabla_s \cdot (\eta\nabla_s\mathbf{u}_s)]\delta l. \quad (14)$$

Further simplifications are achieved under (iii) vanishing grand pressure gradient  $\nabla P_s = 0$ , and (iv) negligible viscous stress for fluid molecules in AL, namely,  $\nabla_s \cdot (\eta \nabla_s \mathbf{u}_s)$ , (14) recovers the generalized Navier boundary condition (5).

It is evident, however, that these criteria are not universally satisfied. For instance, criterion (iii) fails for single-phase Poiseuille flow, while in multiphase systems—where interfacial curvature and viscosity contrasts exist—criterion (iv) does not hold for typical Couette or Stokes flow configurations. Therefore, our model extends the validity of the GNBC by explicitly retaining the viscous and capillary contributions in (14), providing a physically consistent and energetically grounded description of the interfacial slip.

In the subsequent analysis, we apply the present slip model to several representative flow configurations. To highlight the dissipation mechanisms at fluid-solid interfaces with slippage, we employ characteristic material properties of water, namely its viscosity and interfacial tension. Under these conditions, the system exhibits a low Reynolds number ( $\text{Re} \ll 1$ ), ensuring negligible inertial effects. This permits a detailed examination of steady-state solutions that describe interfacial slip and frictional dissipation, enabling a direct comparison with classical theories. Because the focus of this work is on the theoretical formulation and analytical understanding of slip phenomena, we do not include numerical simulations here.

### A. Model Validation

In this part, we consider a simple single-phase flow with confinement to validate the proposed model at steady states with the negligible fluid inertia, so that  $du_s/dt = 0$ . Under this condition, the slip boundary condition (14) is simplified as

$$\lambda \mathbf{u}_s \delta l = \eta \nabla \mathbf{u} \cdot \mathbf{n} - \delta l \nabla P_s.$$

A key distinction from the classical Navier slip boundary condition (NBC) is the presence of the grand pressure-gradient term  $\nabla P_s$ , scaled by the adsorption layer thickness  $\delta l$ , which explicitly enters the interfacial force balance. Such a term has been largely neglected in previous sharp-interface treatments [7, 12, 52]. By explicitly resolving the finite-thickness adsorption layer, our formulation restores a complete local force balance acting on the interfacial region, including both the tangential (parallel) and normal components relative to

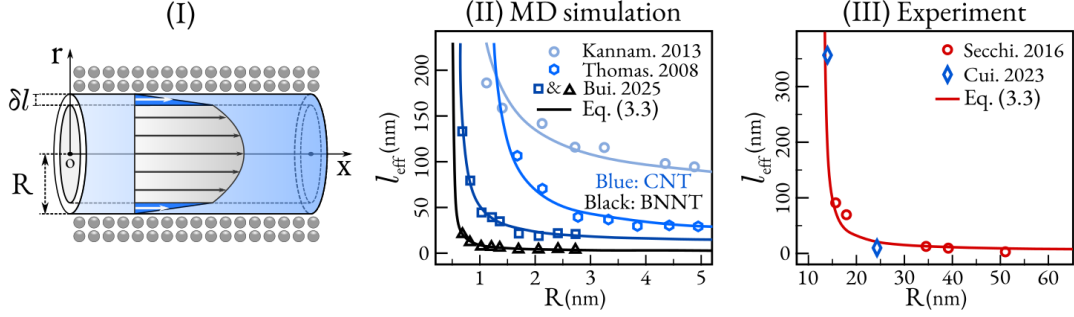


FIG. 3. (I) One-dimensional Poiseuille flow through a tube with radius  $R$ . (II) Calculated effective slip length  $l_{\text{eff}}$  of water in nanotube with (16) shows  $R$ -dependent decays, compared with previous molecular dynamic simulations. CNT: carbon nanotube, BNNT: boron nitride nanotube, for both  $\delta l = 0.5\text{nm}$ . (III) Enhanced experimental slip length of KCl (potassium chloride) aqueous solution ( $10^{-3}\text{M}$ ) in CNT deviates from MD, indicating the larger  $\delta l \approx 13\text{nm}$  associated with the Debye length of KCl solution.

the solid substrate.

For simple incompressible flows, the force balance in normal direction implies

$$(-\nabla P_s - c_s \nabla \mu_s) \cdot \mathbf{n} = 0.$$

Due to the thermodynamic equilibrium for component,  $\nabla \mu_s \cdot \mathbf{n} = 0$ , so that

$$\nabla P_s \cdot \mathbf{n} = 0, \quad (15)$$

per se  $P_s = P$ , indicating that the grand pressure transmitted from the bulk must also act upon the fluid molecules within the AL. Consequently, a pressure gradient persists inside the AL, contributing to fluid motion and playing a crucial role in maintaining mechanical equilibrium. This interfacial condition naturally arises from the energy minimization principle and remains consistent with the entropy production framework [3, 5].

### 1. One-dimensional Poiseuille flow

To further elucidate the physical implications, we first examine the simplest case: a steady Poiseuille flow under confinement in a cylindrical pipe of radius  $R$ , as illustrated in figure 3(I)(i). The velocity field  $\mathbf{u} = (u, 0)$  is axisymmetric and unidirectional along the axial

direction  $x$ . In cylindrical coordinates, the flow satisfies the Stokes equation in the bulk fluid and the force balance in the adsorption layer (AL) described by (12) in AL, namely:

$$\begin{cases} \partial_x P = \nabla \cdot (\eta \nabla \mathbf{u}), & \text{in } r \in [0, R - \delta l], \\ \lambda \mathbf{u}_s \delta l = -\eta \partial_r \mathbf{u} - \delta l \partial_x P_s, & \text{in } r = R - \delta l/2. \end{cases}$$

The first equation represents the Stokes flow in the bulk, while the second expresses the local momentum balance within the adsorption layer (AL). Notably, conventional sharp-interface models [7, 12] neglect the grand pressure-gradient term in the slip boundary condition, thereby decoupling interfacial pressure from that of the bulk. In contrast, following the variational formulation of Bedeaux [3], Qian *et al.* [46], our framework explicitly couples the adsorption-layer pressure with that of the bulk fluid, ensuring thermodynamic and hydrodynamic consistency for AL and the bulk fluid. Due to the pressure coupling between AL and the bulk fluid (15), we have  $\partial_x P_s = \partial_x P$ .

Accounting for this newly added pressure-coupling term, the steady-state velocity profile now becomes

$$\mathbf{u}(r) = \frac{d_x P}{4\eta} [r^2 - (R - \delta l)^2 - 4(R + \delta l)l_s],$$

where  $l_s = \eta/(\lambda \delta l)$  is the intrinsic Navier slip length, characterizing the frictional coupling between the wall and the adjacent fluid molecules. This leads naturally to a confinement-dependent effective slip length, defined as

$$l_{\text{eff}} = \frac{u_s}{\partial_r u} = \left(1 + \frac{2\delta l}{R - \delta l}\right) l_s, \quad (16)$$

which explicitly depends on both the pipe radius and the AL thickness.

Figure 3(II) compares (16) with molecular dynamics (MD) simulations of water flow in carbon nanotubes (CNTs) and boron nitride nanotubes (BNNTs) [7, 28, 53]. The characteristic solid–fluid interaction range is taken as  $\delta l = 0.5\text{nm}$ . For sufficiently large pipes ( $R \gg \delta l$ ), (16) asymptotically recovers the classical Navier slip length,  $l_{\text{eff}} \approx l_s$ , where confinement effects are negligible. At smaller radii, however, our model predicts a pronounced slip enhancement with decreasing  $R$ , in well agreement with MD data. Importantly, our framework also captures the significant difference in slip length between CNTs and BNNTs—despite their nearly identical macroscopic wettability—by attributing it to variations in the interfacial friction coefficient  $\lambda$ . Such variations arise from molecular-scale features

related to the fluid-solid intermolecular bond, such as polarization and surface corrugation, rather than from contact angle differences alone.

We further apply (16) to interpret the extraordinarily large slip lengths observed for electrolytic flows in CNTs, which exceed the values for pure water by several orders of magnitude [14, 50]. In these experiments, a  $10^{-3}\text{M}$  KCl (potassium chloride) solution is used. Without altering other parameters, replacing the characteristic interfacial length by the Debye screening length  $\delta l = 13\text{ nm}$ —representing the ion–solid interaction range—yields theoretical predictions that agree quantitatively with experimental results; see figure 3(III). This demonstrates that electrostatic interactions within the Helmholtz (or Debye) layer can effectively enlarge the hydrodynamic boundary-layer thickness, thus amplifying the apparent slip length. Accordingly, the present model bridges the molecular and continuum descriptions of interfacial slippage, providing a unified interpretation for both neutral and electrolytic confined flows.

Finally, we note that such confinement-induced slip enhancement cannot be reproduced by the classical Navier slip condition, which neglects the thermodynamic coupling between interfacial and bulk pressures. Although [46] introduced a pressure term in their variational force balance, their formulation only addressed the tangential component along the substrate, as the sharp-interface assumption precludes defining the interfacial pressure or its normal balance. In contrast, our adsorption-layer framework restores a physically meaningful interfacial region populated by fluid molecules that remain thermodynamically coupled to the bulk. As a result, while the friction coefficient  $\lambda$  remains an intrinsic property of the solid–fluid bonds, the apparent slip length becomes confinement-dependent due to the pressure coupling. This interpretation differs fundamentally from the confinement-dependent  $\lambda$  hypothesis proposed by [7]. We emphasize that  $\lambda$  reflects the intrinsic strength of intermolecular bonding rather than flow geometry; its apparent variation arises indirectly through the pressure-mediated interaction between the bulk fluid and the AL.

## 2. *Two-dimensional Poiseuille flow*

When the curvature of the geometry is neglected—for example, in two-dimensional Poiseuille flow between parallel plates separated by a distance  $2H$ —the effective slip length

takes

$$l_{\text{eff}} = \left(1 + \frac{\delta l}{H - \delta l}\right) l_s. \quad (17)$$

This expression indicates that as the confinement becomes stronger  $H \rightarrow \delta l$ , the slip length increases due to the increased contribution of interfacial slippage relative to the total height of the channel. This confinement-induced enhancement was not captured in MD simulations [7], where a geometry-independent slip length is prescribed as a constant value.

Based on (17), the corresponding effective interfacial friction coefficient follows directly from the Navier definition by (3),

$$\lambda_{\text{eff}} = \frac{\eta}{l_{\text{eff}}} = \frac{H - \delta l}{H} \lambda_{\text{intr}}, \quad (18)$$

where  $\lambda_{\text{intr}} = \eta/l_s$  denotes the intrinsic interfacial friction coefficient. In the limit  $H \rightarrow \infty$ , (18) converges to the bulk value, as expected. This scaling differs from the prediction of the classical hydrodynamic theory (CHT) [7], which yields

$$\lambda_{\text{eff,CHT}} = \frac{6\eta}{H + 3l_s}, \quad (19)$$

implying that the effective friction vanishes for very large channel heights ( $H \rightarrow \infty$ ). Our formulation, in contrast, captures the finite friction resistance sustained by the interfacial layer even in wide channels, highlighting the physical role of the adsorption layer thickness  $\delta l$  in modulating momentum transfer.

### 3. Couette Flow

We next consider the two-dimensional Couette flow confined between two parallel plates separated by a distance  $H$ . The upper plate moves with constant velocity  $U_0$  at  $h = H$ , while the lower plate remains stationary at  $h = 0$ . Within the bulk, the velocity field satisfies the Stokes equation with a uniform shear rate, whereas the momentum balance in the adsorption layer (AL) introduces a velocity jump governed by the frictional coupling at each wall. The analytical solution of the steady velocity profile reads

$$u(h) = U_0 \frac{h + 2l_s - \delta l}{H + 4l_s - 2\delta l}, \quad (20)$$

which reduces to the classical linear Couette profile in the limit  $\delta l \rightarrow 0$ , confirming consistency with the no-slip condition. The corresponding effective slip length evaluated at the

wall interface is  $l_{\text{eff}} = l_s$ , indicating that, unlike the Poiseuille configuration, the Couette flow does not exhibit geometric dependence of the slip length on the confinement spacing  $H$ .

## B. Surface Depletion/Adsorption Effect

In multicomponent fluid systems, the solid substrate may preferentially adsorb or deplete one component, leading to a surface composition that deviates from the bulk mixture. This compositional gradient along the substrate normal direction induces a spatially varying viscosity field, thereby altering the local hydrodynamics within AL. Considering the normal force balance in AL, we have

$$\nabla P_s \cdot \mathbf{n} = c_s \nabla \mu_s \cdot \mathbf{n} = 0.$$

whose solution gives rise to the steady-state concentration profile following an exponential relaxation, depending on the surface depletion/adsorption [57]. Thus, the viscosity distribution in the 1D Poiseuille flow can be approximated as

$$\eta(r) = 1 + \eta_0 e^{R/\delta l} \cosh(r/\delta l),$$

where  $\eta_0$  characterizes the magnitude of viscosity modulation induced by surface adsorption or depletion. Substituting this expression into the momentum balance yields the steady velocity profile,

$$u(r) = -\frac{1}{2} \int_0^r \frac{s \, dP/dx + C_1}{1 + \eta_0 e^{R/\delta l} \cosh(s/\delta l)} \, ds + C_2,$$

where the integration constants  $C_1, C_2$  are decided by slip boundary conditions at wall.

By varying  $\eta_0$ , the resulting viscosity and velocity distributions are depicted in figure 4(I)-(II). For  $\eta_0 > 0$ , the local viscosity near the wall increases due to surface adsorption, producing a pronounced suppression of the near-wall velocity. Conversely,  $\eta_0 < 0$ , corresponds to surface depletion, reducing viscosity near the wall and thereby enhancing the flow velocity within the AL region.

Interestingly, when evaluating the effective slip length from the velocity gradient using Navier's definition of (16), the computed  $l_{\text{eff}}$  appears larger for the more viscous (adsorptive) case, as shown in figure 4(III). This seemingly counterintuitive trend arises because a steeper velocity gradient  $\partial u/\partial r$  develops near the fluid-solid interface when the local viscosity increases, thereby inflating the apparent slip length defined through this ratio.

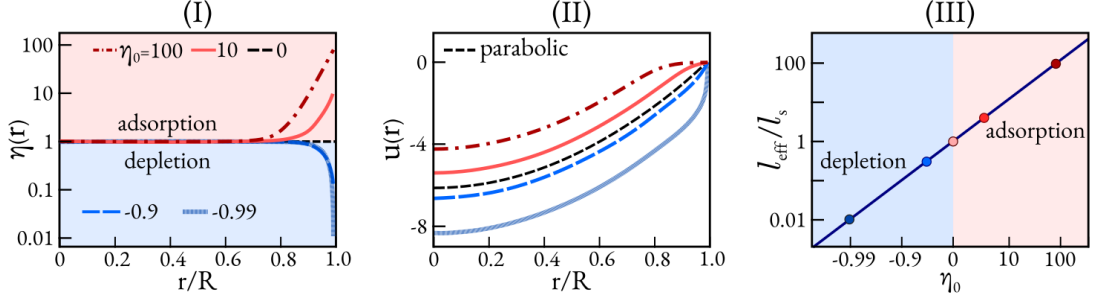


FIG. 4. One-dimensional Poiseuille flow with surface depletion/adsorption. Tube radius  $R = 50$ , characteristic length  $\delta l = 0.5$ , friction coefficient  $\lambda = 20$ . (I) Depletion/adsorption induced viscosity distribution  $\eta(r) = 1 + \eta_0 e^{R/\delta l} \cosh(r/\delta l)$ .  $\eta_0 > 0$ : adsorption increases viscosity;  $\eta_0 < 0$ : depletion reduces viscosity. (II) Flow profile modified by surface depletion/adsorption. Black line: parabolic profile without depletion/adsorption. (III) Effective slip length  $l_{\text{eff}}$  changing with depletion/adsorption; dots: (16), line: linear relation.

This observation reveals a fundamental limitation of using “slip length” as a universal descriptor of interfacial hydrodynamics. The parameter  $l_{\text{eff}}$  does not always reflect a genuine slip phenomenon but rather encodes the combined effects of interfacial friction, local viscosity variation, and flow geometry. A more physically meaningful characterization should therefore rely on the explicit interfacial parameters—namely, the local viscosity  $\eta(c, r)$  and the friction coefficient  $\lambda$ —instead of prescribing or inferring a single slip length. Such an approach avoids the ambiguity of interpreting  $l_{\text{eff}}$  in complex or compositionally heterogeneous systems.

As the velocity profile  $u(r)$  is modified by the local viscosity variations caused by surface adsorption or depletion, the volumetric flow rate through the cylindrical conduit is obtained by integrating the velocity field,

$$Q = \int_0^R 2\pi r u(r) dr.$$

This expression deviates from the standard Poiseuille flow rate,  $Q_s$ , associated with a uniform viscosity and Navier slip boundary condition [33],

$$Q_s = Q_0 \left( 1 + \frac{4l_s}{R} \right), \quad (21)$$

where  $Q_0 = -\pi R^4 d_x P / (8\eta)$  is the classical no-slip flow rate. (21) corresponds to a special case of our model with  $\eta_0 = 0$ , i.e., uniform composition without adsorption layer effects.

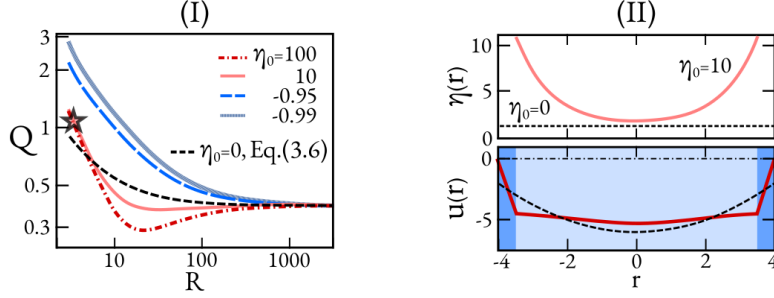


FIG. 5. (I) Flow rate of one-dimensional Poiseuille flow with slip influenced by surface depletion/adsorption for different tube radius  $R$ . The black dashed line: standard  $Q_s$  by (21). (II) Viscosity  $\eta$  and flow velocity  $u(r)$  deviate from the standard Poiseuille flow without surface adsorption (dashed black lines), for small confinement with  $R = 4$ , corresponding to the star symbol in (I). The dark blue and light blue regions denote AL and bulk fluid, respectively.

Figure 5(I) compares the normalized flow rate  $Q/Q_s$  under various conditions of surface depletion/adsorption. When surface depletion leads to a local viscosity reduction near AL ( $\eta_0 < 0$ ), the flow rate increases monotonically relative to  $Q_s$  and gradually approaches the standard Poiseuille value as the tube radius increases. Conversely, for  $\eta_0 > 0$ , where adsorption enhances the viscosity near the wall, the flow rate exhibits a non-monotonic dependence on the confinement radius  $R$ . At small confinements ( $R = 4$ ), as shown in figure 5(II), the velocity profile becomes flattened near the channel centerline and elevated within the adsorption layer, deviating markedly from the classical parabolic profile (black dashed line). This counterintuitive enhancement of flow at small  $R$  arises because, within the adsorption layer, the viscous drag force dominates over the interfacial frictional resistance, thereby producing an increased slip velocity despite a locally higher viscosity. Although in all configurations the prescribed effective slip length  $l_s = 1.0$  is held constant, the modified near-wall viscosity distribution alters the apparent flow enhancement, demonstrating that the same  $l_s$  can correspond to different global transport rates.

Consequently, using the standard relation in (21) to infer slip length from measured flow rates may lead to significant over- or under-estimation, depending on the degree of surface adsorption or depletion. This sensitivity highlights the non-universality of the slip length concept when viscosity varies spatially near the interface. MD simulations of pure water slippage indeed reveal a viscosity deviation from the bulk value within several molecular diameters of the solid surface. In experimental studies involving multicomponent fluids, even

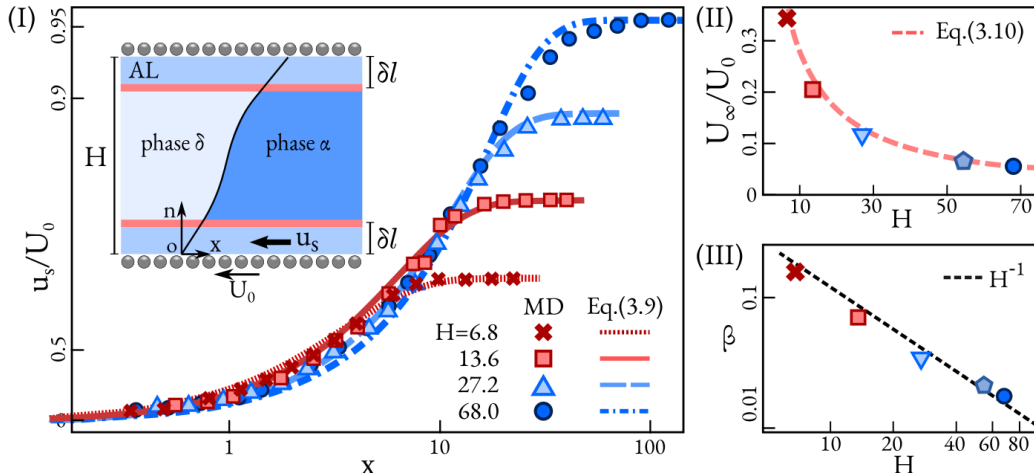


FIG. 6. (I) Flow velocity  $u_s$  in AL from the triple junction  $x = 0$ . Open-colored symbols:  $u$  by molecular dynamics simulation from Qian *et al.* [46]. Colored curves: theory with (23). Inset: flow setup. (II) Far field flow velocity  $U_\infty$  in AL fulfills Couette flow with (24). (III) Fitting parameter  $\beta$  scaling with the plane spacing  $H$ . Colored symbols in (II)(III) correspond to the markers in (I).

when perfectly smooth substrates are used, such near-wall viscosity variations can substantially affect the hydrodynamic response. Hence, the conventional practice of determining  $l_s$  via (21) should be re-examined; accurate characterization of slip requires accounting for composition-dependent viscosity fields and adsorption layer dynamics.

### C. Wedge flow

In the previous section, we analyzed single-phase confined flows, highlighting how slip-page arises from the coupling between the bulk fluid and the adsorption layer. There, the pressure-gradient term and surface composition were shown to play crucial roles through their thermodynamic equilibrium in the direction normal to the fluid-solid interface, indirectly modulating the slip velocity. We now extend our analysis to a two-phase configuration—the  $\alpha - \delta$  system—forming a wedge-shaped flow near the moving contact line, as illustrated in the inset of figure 6(I).

First analyzed by Huh & Scriven [25], they assumes that the wedge flow is constraint by the no-slip boundary condition, while neglecting local force balance near the contact line. Solving the Stokes equation in polar coordinates  $(r, \phi)$ , their model leads to the well-known Huh–Scriven paradox, in which the viscous stress diverges as  $r \rightarrow 0$ . Later studies resolved

this paradox by introducing microscopic interfacial effects. Similarly, [12, 23] employed the Navier slip condition to regularize the stress singularity, while Shikhmurzaev [51] introduced a surface composition–dependent slip model to achieve a comparable effect. Qian *et al.* [46] and Yue *et al.* [65] showed numerically that the paradox disappears once the liquid–liquid interface is treated as a diffuse region with finite thickness, ensuring that  $r$  never strictly vanishes. Building on these developments, we revisit the velocity distribution near the triple junction by incorporating the viscous stress term  $\nabla_s \cdot (\eta \nabla_s \mathbf{u}_s) \delta l$  in (14) that naturally arises from our adsorption-layer formulation—yet has been overlooked in prior treatments. Using the parameters of Qian *et al.* [46], we compare our analytical predictions against molecular dynamics results for validation.

### 1. Velocity Profile in Adsorption Layer

Following the setup of Qian *et al.* [45, 46], we consider a two-dimensional Couette-type flow where the lower substrate moves with velocity  $U_0$ . Both fluid phases are assumed to have identical viscosities, such that the velocity field is symmetric about  $x = 0$ . Hence, only the right-hand phase ( $\alpha$ , with  $x > 0$ ) is analyzed. In this configuration, no externally imposed pressure gradient exists as in Poiseuille flow. Instead, the Laplace pressure gradient  $-\nabla p$  is balanced by the thermodynamic driving force  $-c_s \partial_x \mu_s$  at steady state, particularly when the slip velocity remains small. Thus, the grand pressure gradient  $\nabla P_s$  becomes negligible. Under these assumptions, the momentum balance in the AL (14) reduces to

$$\lambda(u_s - U_0) \delta l = \eta \frac{\partial^2 u_s}{\partial x^2} \delta l + \eta \frac{\partial u}{\partial n}. \quad (22)$$

Far from the contact line ( $x \gg 1$ ), the viscous stress term  $\eta \partial_{xx} u$  becomes negligible, and the flow transitions into a quasi–Couette regime. Near the contact line, however, the slip velocity decreases sharply and the fluid within the AL becomes nearly stagnant, indicating a finite viscous stress contribution that cannot be ignored. This slip velocity gradient in substrate tangent direction is also scaled by AL thickness  $\delta l$ , which reveals that friction and viscous coupling act over a finite length scale, rather than at a singular boundary.

At the far field ( $x \rightarrow \infty$ ), the slip velocity approaches the asymptotic value  $u_s(\infty) = U_\infty$ , which is determined by the Couette flow expression (20). Assuming that the near-contact-line flow is generated by this Couette motion, we approximate the viscous traction term

in (22) as  $\eta\partial_n u \simeq \nu(u_s - U_\infty)$ , where  $\nu$  is a geometry-dependent scaling parameter extracted from MD simulations. Substituting into (22) gives an exponentially decaying slip-velocity profile within the AL:

$$u_s(x) = (U_c - U_\infty)e^{-\beta x} + U_\infty, \quad (23)$$

where  $U_c$  denotes the slip velocity at the contact line. The decay rate  $\beta = \sqrt{(\lambda + \nu)/\eta}$  depends on the flow geometry and exhibits a power-law scaling with the channel height  $H$ , as shown by the log–log plot in figure 6(III).

Figure 6(I) compares our analytical prediction from (23) with the MD simulation data of Qian *et al.* [46], demonstrating excellent agreement. This result underscores the importance of the viscous term  $\nabla_s \cdot (\eta\nabla_s u_s)\delta l$ , which induces an inhomogeneous slip velocity along the fluid–solid interface. Our formulation therefore complements the interface-formation model of [51], where slip heterogeneity is attributed solely to variations in surface composition. In contrast, our model—and the MD results of Qian *et al.* [44]—show that even in the absence of compositional gradients, viscous effects within the AL can produce comparable slip variations. Finally, the far-field slip velocity is given by

$$U_\infty = U_0 \frac{2\delta l}{H + 2\delta l}, \quad (24)$$

which matches the single-phase Couette flow prediction in (20), as shown in figure 6(II). This consistency confirms that, in the far field, the same interfacial mechanisms governing single-phase flow remain valid near the moving contact line when the adsorption layer is properly accounted for.

In this analysis, we assume equal viscosities for both fluid phases, consistent with [46]. If the viscosities differ, however, the term  $\nabla_s \cdot (\eta\nabla_s u_s)\delta l$  becomes even more significant in the interfacial force balance, leading to pronounced variations in slippage and slip velocity. Such cases cannot be solved analytically and will require numerical investigation, which will be pursued in our future work.

#### IV. CONCLUSION

In this work, we investigate the fundamental physical mechanisms underlying slip boundary condition by examining the coupled hydrodynamic and thermodynamic behaviors of

multicomponent fluids in contact with solid substrates. We introduced the concept of an adsorption layer (AL), treating the fluid–solid interface not as a mathematically sharp boundary but as a finite interfacial region where molecular interactions govern both mass transport and momentum exchange. Within this layer, solid–fluid interactions not only drive adsorption/depletion—minimizing chemical free energy, but also induce interfacial flows that dissipate kinetic energy.

By applying energy minimization principles, we established a general force-balance framework within the AL that couples thermodynamic and hydrodynamic effects. A central outcome is the identification of solid–fluid friction as the key factor controlling slippage. At the molecular level, this friction originates from the elongation, contraction, and rotation of interfacial bonds that resist tangential motion, linking the macroscopic frictional force to the microscopic bonding energy between solid and fluid molecules. The AL thus acts as a transitional zone where energy dissipation occurs through both hydrodynamic via momentum transfer and thermodynamic surface diffusion and convection.

We validated this framework in classical flow configurations—including Poiseuille, Couette, and wedge flows—and demonstrated that slip arises as a self-consistent interfacial property. It depends not only on the interplay between interfacial friction and fluid viscosity in the tangential direction, but also on thermodynamic coupling across the interface normal, which is typically neglected in sharp-interface models. This coupling naturally explains phenomena such as confinement-enhanced water slippage in carbon nanotubes, which cannot be captured by conventional approaches. In this picture, the “slip length” is no longer a prescribed parameter, but an emergent, spatially varying quantity determined by local friction, viscous drag, and surface composition.

Together, these results establish a unified framework that links microscopic friction within the adsorption layer to macroscopic interfacial motion, bridging molecular-scale physics with continuum-scale hydrodynamics. Looking forward, several directions are promising. Incorporating temperature gradients could capture thermally driven slip and Marangoni effects, while extending the theory to electrokinetic systems may reveal charge-mediated wetting dynamics.

## FUNDINGS

This work was supported by the Gottfried-Wilhelm Leibniz prize NE 822/31-1 of the German research foundation (DFG), VirtMat project P09 “Wetting Phenomena” of the Helmholtz Association (MSE-programme No. 43.31.01).

## DECLARATION OF INTERESTS

The authors report no conflict of interest.

## Appendix A: Total energy functional and governing equation

Considering the multi-component system with droplets that contact the solid substrate, the *fluid* has the total energy density functional  $\mathcal{L}$  consisting of three parts, namely, the chemical free energy functional  $\mathcal{F}$ , the potential energy  $\mathcal{P}$ , and the kinetic energy  $\mathcal{K}$ ,

$$\mathcal{L} = \mathcal{F} + \mathcal{P} + \mathcal{K}.$$

In addition, the kinetic energy of the *solid substrate*  $\mathcal{K}_w$  should also be considered. Thus, the total energy density functional of the fluid and substrate system reads

$$\mathcal{L}_T = \mathcal{L} + \mathcal{K}_w.$$

### 1. Chemical free energy functional

The fluid chemical free energy functional  $\mathcal{F}$  is formulated as the summation of the bulk free energy functional ( $\mathcal{F}_b$ ) in the bulk fluid domain  $\Omega$ , and the wall energy functional ( $\mathcal{F}_s$ ) at the fluid-solid contact surface  $S$  as

$$\mathcal{F} = \mathcal{F}_b + \mathcal{F}_s = \int_{\Omega} g \, d\Omega + \int_S g_w \, \delta l \, dS.$$

Especially, in this work, we specify the thin layer in the fluid-solid contact region with thickness  $\delta l$  and denominate it as the adsorption layer (AL). This thin layer denotes the region where solid and fluid interactions exist, resulting in the adsorption and depletion of the fluid molecules. For different fluid-solid pairs, the magnitude of  $\delta l$  ranges from several nanometer to micro-meter scales [8, 55], which depends not only on the properties of the fluid solid interactions, but also on the size of the molecules.

*a. Chemical Free Energy in Bulk Fluids*

The bulk free energy density functional  $g(\mathbf{c}, \nabla \mathbf{c})$  takes the Cahn-Hilliard formulation [9, 66]

$$g = f(\mathbf{c}) + \sum_i \kappa (\nabla c_i)^2 / 2,$$

in which the spatial-temporal fluid composition is defined by  $\mathbf{c}(\mathbf{x}, t) = (c_1, c_2, \dots, c_i, \dots)$  and  $f$  is the bulk free energy density which is a function of  $\mathbf{c}(\mathbf{x}, t)$ .

*b. Chemical free energy in AL*

In  $\mathcal{F}$ , the second integrand  $g_w(\mathbf{c}_s, \nabla \mathbf{c}_s)$  scales the chemical interaction between the fluid and the solid substrate, and is related with the combination of entropy density  $s_w$ , enthalpy density  $h_w$  and van der Waals interaction  $f_{\text{vdW}}$  [16, 56] as,

$$f_w = h_w(\mathbf{c}) - T s_w(\mathbf{c}) + f_{\text{vdW}}.$$

Noteworthy,  $f_{\text{vdW}}$  between solid and fluid molecules alters the free energy of fluid molecules and can be calculated with the Lennard-Jones type of potential energy density as

$$f_{\text{vdW}} = \sum_i \epsilon c_i [(\sigma_i/r_0)^m - (\sigma_i/r_0)^n],$$

where  $\epsilon$  is the depth of the potential well and  $\sigma_i$  is the distance at which the potential energy is zero. The scaling parameters  $m$  and  $n$  are obtained from experiments. Apparently, we assume that the total van der Waals force is composition dependent. In this way, the wall energy density also depends on the surface composition, namely  $f_w(\mathbf{c}_s)$  which differs from the bulk free energy density  $f(\mathbf{c})$ . By defining the AL thickness  $\delta l$  as the characteristic length scale of the solid-fluid intermolecular forces, the total chemical free energy functional is formulated with

$$\mathcal{F} = \int_{\Omega} \left[ f(\mathbf{c}) + \sum_i \kappa (\nabla c_i)^2 / 2 \right] d\Omega + \int_S \left[ f_w(\mathbf{c}_s) + \sum_i \kappa_s (\nabla c_{s,i})^2 / 2 \right] \delta l dS.$$

## 2. Potential energy and kinetic energy

For the multi-component fluid flow, the potential energy of the fluid is represented by

$$\mathcal{P} = \mathcal{P}_b + \mathcal{P}_s = \int_{\Omega} p d\Omega + \int_S p_s \delta l dS.$$

Here, the pressure density in bulk and AL are labeled by  $p$  and  $p_s$ , respectively. The fluid kinetic energy takes the following formulation with the macroscopic fluid velocity  $\mathbf{u}$  inside the bulk region, and  $\mathbf{u}_s$  in AL,

$$\mathcal{K} = \mathcal{K}_b + \mathcal{K}_s = \int_{\Omega} \frac{\rho \mathbf{u}^2}{2} d\Omega + \int_S \frac{\rho \mathbf{u}_s^2}{2} \delta l dS,$$

where the density  $\rho$  is assumed to be constant.

### 3. Evolution equations by energy minimization

#### a. Chemical Free Energy dissipation

From the temporal decay of the chemical free energy functional  $\mathcal{F}$ , we have

$$d\mathcal{F}/dt = \int_{\Omega} \sum_i \left[ \frac{\delta g}{\partial c_i} \frac{dc_i}{dt} + \nabla \cdot (\kappa \nabla c_i \otimes \nabla c_i) \cdot \mathbf{u} \right] d\Omega \quad (\text{A1})$$

$$+ \int_S \sum_i \left[ \frac{\delta g_w}{\partial c_{s,i}} \frac{dc_{s,i}}{dt} + \nabla \cdot (\kappa_s \nabla c_{s,i} \otimes \nabla c_{s,i}) \cdot \mathbf{u}_s \right] \delta l dS. \quad (\text{A2})$$

The second integrand in (A1) is obtained from the divergence theorem and the equality of vector calculus  $\nabla \cdot (\mathbf{a} \otimes \mathbf{b}) = \nabla \cdot (\mathbf{a}) \mathbf{b} + \mathbf{a} \cdot \nabla \mathbf{b}$ . Physically, Eqs. (A1) and (A2) describe the dissipation of chemical free energy via bulk diffusion and surface diffusion in AL, respectively.

### 4. Kinetic energy dissipation

The kinetic energy dissipation is calculated with the total derivatives as,

$$d\mathcal{K}/dt = \int_{\Omega} \rho \mathbf{u} \cdot d\mathbf{u}/dt d\Omega + \int_S \rho \mathbf{u}_s \cdot d\mathbf{u}_s/dt \delta l dS. \quad (\text{A3})$$

### 5. Potential energy dissipation

The potential energy dissipation follows the simple chain rule,

$$d\mathcal{P}/dt = \int_{\Omega} \frac{dp}{d\mathbf{x}} \cdot \frac{d\mathbf{x}}{dt} d\Omega + \int_S \frac{dp_s}{d\mathbf{x}} \cdot \frac{d\mathbf{x}}{dt} \delta l dS = \int_{\Omega} \nabla p \cdot \mathbf{u} d\Omega + \int_S \nabla p_s \cdot \mathbf{u}_s \delta l dS. \quad (\text{A4})$$

## 6. Governing equations in bulk fluids

Collecting the bulk total energy dissipation terms in (A2) (A3) (A4), we have

$$\frac{d\mathcal{L}_b}{dt} = \frac{d(\mathcal{F}_b + \mathcal{K}_b + \mathcal{P}_b)}{dt} = \int_{\Omega} \left\{ \sum_i \frac{\delta g}{\delta c_i} \frac{dc_i}{dt} + \left[ \sum_i \nabla \cdot (\kappa \nabla c_i \otimes \nabla c_i) + \nabla p + \rho \frac{d\mathbf{u}}{dt} \right] \cdot \mathbf{u} \right\} d\Omega. \quad (\text{A5})$$

We easily obtain the evolution equations by the energy dissipation in bulk fluid—the Cahn-Hilliard-Navier-Stokes model (CHNS), or the so-called model H,

$$\begin{aligned} \nabla \cdot \mathbf{u} &= 0, \\ \partial c_i / \partial t + \mathbf{u} \cdot \nabla c_i &= \nabla \cdot (M \nabla \mu_i), \\ \rho d\mathbf{u}/dt &= -\nabla \cdot (\mathbf{P}\mathbf{I} + \underline{\underline{\Theta}}) + \nabla \cdot \underline{\underline{\sigma}}. \end{aligned} \quad (\text{A6})$$

The first equation denotes the incompressibility. The second evolves the composition in bulk in which the bulk chemical potential is defined with  $\mu_i = \delta g / \delta c_i = \partial f / \partial c_i - \kappa \nabla^2 c_i$ . The mobility  $M$  scales the bulk diffusion which follows the Onsager's relation; more details in our previous work [69]. The third equation describes the force balance on the fluid takes the tensor formation, which contains the grand pressure  $P$ , the surface stress tensor  $\underline{\underline{\Theta}}$ , and viscous stress tensor  $\underline{\underline{\sigma}}$ ,

$$P = p + g - \sum_i \frac{\delta g}{\delta c_i} c_i, \quad \underline{\underline{\Theta}} = -\left(g - \sum_i \frac{\delta g}{\delta c_i} c_i\right) \mathbf{I} + \sum_i \kappa \nabla c_i \otimes \nabla c_i, \quad \underline{\underline{\sigma}} = \eta (\nabla \mathbf{u} + \nabla \mathbf{u}^T).$$

If not written in the tensor form, the force balance equation can also be expressed as

$$\rho d\mathbf{u}/dt = -\nabla P - \sum_i c_i \nabla \mu_i + \nabla \cdot [\eta (\nabla \mathbf{u} + \nabla \mathbf{u}^T)].$$

Substituting (A6) into (A5), the total energy dissipation in bulk fluid obeys,

$$d\mathcal{L}_b/dt = - \int_{\Omega} \left[ \sum_i M (\nabla \mu_i)^2 + \eta \nabla \mathbf{u} : \nabla \mathbf{u} \right] d\Omega. \quad (\text{A7})$$

## 7. Governing equations in adsorption layer

Next, we focus on deducing the feasible force balance equation in AL. Still, the skeleton key is the total energy minimization.

$$\frac{d\mathcal{L}_s}{dt} = \int_S \left\{ \sum_i \frac{\delta g_w}{\delta c_{s,i}} \frac{dc_{s,i}}{dt} + \left[ \sum_i \nabla \cdot (\kappa_s \nabla c_{s,i} \otimes \nabla c_{s,i}) + \nabla p_s + \rho \frac{d\mathbf{u}_s}{dt} \right] \cdot \mathbf{u}_s \right\} dl dS. \quad (\text{A8})$$

The derivation is similar to the bulk fluid, but with only one difference. The friction force between fluid and solid substrate needs to be considered in the force balance equation in AL,

$$\nabla \cdot \mathbf{u}_s = 0,$$

$$\partial c_{s,i}/\partial t + \mathbf{u}_s \cdot \nabla c_{s,i} = \nabla \cdot (M_s \nabla \mu_{s,i}), \quad (\text{A9})$$

$$\rho \, d\mathbf{u}_s/dt = -\nabla \cdot (\mathbf{P}_s \mathbf{I} + \underline{\underline{\Theta}}_s) + \nabla \cdot \underline{\underline{\sigma}}_s - \lambda(\mathbf{u}_s - \mathbf{u}_w),$$

where the surface chemical potential is defined with  $\mu_{s,i} = \delta g_w / \delta c_{s,i} = \partial f_w / \partial c_{s,i} - \kappa \nabla^2 c_{s,i}$ . The mobility  $M_s$  scales the surface diffusion. The stress tensors are defined with the same formulations as the bulk fluids,

$$\mathbf{P}_s = p_s + g_w - \sum_i (\delta g_w / \delta c_{s,i}) c_{s,i}, \quad \underline{\underline{\sigma}}_s = \eta (\nabla \mathbf{u}_s + \nabla \mathbf{u}_s^T),$$

$$\underline{\underline{\Theta}}_s = -[g_w - \sum_i (\delta g_w / \delta c_{s,i}) c_{s,i}] \mathbf{I} + \sum_i \kappa \nabla c_{s,i} \otimes \nabla c_{s,i}.$$

If not written in the tensor form, the force balance in AL is expressed as

$$\rho \frac{d\mathbf{u}_s}{dt} = -\nabla p_s - \sum_i c_{s,i} \nabla \mu_{s,i} + \nabla \cdot [\eta (\nabla \mathbf{u}_s + \nabla \mathbf{u}_s^T)] - \lambda(\mathbf{u}_s - \mathbf{u}_w),$$

which recovers the expression we applied in this work.

## 8. Energy dissipation

Substituting (A9) into (A8), the total surface energy dissipation in AL obeys,

$$\frac{d\mathcal{L}_s}{dt} = - \int_{\Omega} \left[ \sum_i M_s (\nabla \mu_{s,i})^2 + \eta \nabla \mathbf{u}_s : \nabla \mathbf{u}_s + \lambda(\mathbf{u}_s - \mathbf{u}_w) \cdot \mathbf{u}_s \right] \delta l \, dS. \quad (\text{A10})$$

This term is not always negative, because the fluid-solid friction can do work on fluid and can either accelerate, or decelerate the fluid. So we shall not forget the power made by the solid-fluid friction onto the *solid substrate*, namely

$$\frac{d\mathcal{K}_w}{dt} = \int_S -\mathbf{F} \cdot \mathbf{u}_w \, \delta l \, dS = \int_S \lambda (\mathbf{u}_s - \mathbf{u}_w) \cdot \mathbf{u}_w \, \delta l \, dS.$$

Combining  $d\mathcal{L}/dt$  with  $d\mathcal{K}_w/dt$ , the total energy functional of the *multicomponent fluid and solid substrate* dissipates with time as,

$$\begin{aligned} \frac{d\mathcal{L}_T}{dt} = \frac{d(\mathcal{L}_b + \mathcal{L}_s + \mathcal{K}_w)}{dt} &= - \int_{\Omega} [\sum_i M (\nabla \mu_i)^2 + \eta \nabla \mathbf{u} : \nabla \mathbf{u}] \, d\Omega \\ &\quad - \int_S [\sum_i M_s (\nabla \mu_{s,i})^2 + \eta \nabla \mathbf{u}_s : \nabla \mathbf{u}_s + \lambda(\mathbf{u}_s - \mathbf{u}_w)^2] \, \delta l \, dS \leq 0 \quad \blacksquare \end{aligned}$$

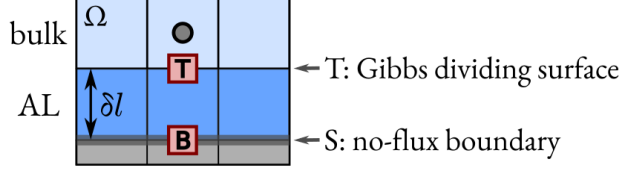


FIG. 7. Discretization of the bulk domain  $\Omega$  and adsorption layer (AL).

The first integral in domain  $\Omega$  denotes the energy dissipation in bulk fluids via diffusion and fluid viscous effect. The second integral in AL highlights the three feasible energy minimizing mechanisms, namely, the surface diffusion (depletion/adsorption), the fluid viscous effect, and the solid-fluid friction.

### Appendix B: Composition Evolution Equation in Adsorption Layer

Inside AL, we use the Cahn-Hilliard type the composition conservation equation,

$$\frac{dc_s}{dt} = \nabla \cdot (M_s \nabla \mu_s), \quad (\text{B1})$$

which is different from the non-conserved form used by [26, 46, 51, 65] as

$$\frac{d\tilde{c}_s}{dt} = -\tau \tilde{\mu}_s, \quad (\text{B2})$$

where the surface chemical potential in the sharp interface model  $\tilde{\mu}_s$  is introduced as a pure mathematic concept with the unit of  $\text{J}/\text{m}^2$ . While the chemical potential in the present AL approach now has a clear physical meaning which is related to the interacting solid and fluid molecules and has the unit of  $\text{J}/\text{m}^3$ . The composition in the sharp interface model  $\tilde{c}_s$  has the relation with our clearly defined surface composition  $c_s$  as  $\tilde{c}_s = c_s \delta l$ .

#### 1. Wetting boundary condition revisit

In the following parts, we proof that the conventional non-conserved wetting boundary condition (B2) is only a numerical approach which is a simplification of our model. First, we discretize the diffusion flux in adsorption layer into the substrate normal (n) and tangential (t) directions, respectively,

$$\frac{dc_s}{dt} = \nabla_n \cdot (M_s \nabla_n \mu_s) + \nabla_t \cdot (M_s \nabla_t \mu_s). \quad (\text{B3})$$

*Ansatz 1:* If we neglect the diffusion flux in the substrate tangential direction, and let the surface mobility  $M_s$  to be a constant independent on the surface composition, the material conservation equation is simplified as

$$\frac{dc_s}{dt} = \nabla_n \cdot (M_s \nabla_n \mu_s) = \frac{M_s \nabla_n \mu_s^T - M_s \nabla_n \mu_s^B}{\delta l},$$

in which the fluxes at top, bottom are positioned at the colored squares in figure 7 and represented by T, B, respectively. Noting the no flux boundary condition at the real solid-fluid interface (position B),

$$\frac{dc_s}{dt} = \frac{M_s}{\delta l} \nabla_n \mu_s^T = -\frac{M_s}{\delta l^2} (\mu_s - \mu^\circ),$$

where  $\mu^\circ$  is the chemical potential of the cell above AL, depicted by the black dot in figure 7.

*Ansatz 2:* Neglecting the thermodynamical coupling between AL and the bulk fluid by chemical potential with  $\mu^\circ = 0$ , we have

$$\frac{dc_s}{dt} = -\frac{M_s}{\delta l^2} \left[ \frac{\kappa_s \nabla_n c_s^T}{\delta l} + \nabla_t \cdot (\kappa_s \nabla_t c_s) - \frac{\partial f_w}{\partial c_s} \right].$$

*Ansatz 3:* Neglecting the surface tangential diffusion with  $\nabla_t \cdot (\kappa_s \nabla_t c_s) = 0$ , the standard non-conserved Allen-Cahn type of wetting boundary condition [11, 18, 26, 58, 65] is recovered from the conserved Cahn-Hilliard formulation,

$$\frac{dc_s}{dt} = -\frac{M_s}{\delta l^3} \left( \kappa_s \nabla_n c_s^T - \delta l \frac{\partial f_w}{\partial c_s} \right) = -\tau \left( \kappa \nabla c_s \cdot \mathbf{n} - \frac{\partial \gamma}{\partial c_s} \right). \quad (\text{B4})$$

where the term  $\gamma(c_s) := f_w(c_s) \delta l$  is understood as the solid-fluid interfacial tension which is a function of  $c_s$ . Hence, the so-called phenomenological kinetic parameter  $\tau$  in previous models has a concrete physical definition as

$$\tau = M_s / \delta l^3,$$

which scales the diffusion flux of fluid molecules entering the adsorption layer from the bulk region through the surface T, due to the unbalanced chemical potential. Besides,  $\tau$  shows a clear relationship with the characteristic length scale  $\delta l$  which denotes the range of solid-fluid chemical interactions.

It needs to be stress that Ansatz 2 is not always true for many systems, even when the equilibrium of AL is reached. Actually, the static state indicates the equal chemical potential

$$\mu_s - \mu^\circ = \nabla \mu_s \cdot \mathbf{n} \Big|_{\text{T}} = 0,$$

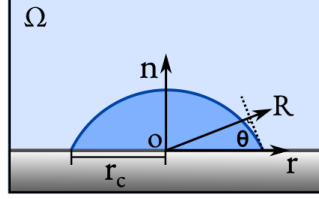


FIG. 8. Sessile droplet on the substrate.  $r_c$  is the contact line radius,  $R$  is the normal direction of the droplet-air surface.

which is the real no-flux boundary condition at the position T. However, the Allen-Cahn type of wetting boundary condition (B4) is a special case which only leads to  $\mu_s = \mu^o = 0$  at equilibrium states. (B4) works well for the droplet wetting and hydrodynamic scenarios, because of its subtle influence compared with the strong hydrodynamics. However, the constraint  $\mu_s = \mu^o = 0$  is not always thermodynamically consistent.

Easily picking a counterexample, for the 1 : 1 binary electrolyte with initial composition  $c_0$ , the equilibrium electrochemical potential of the ions in HDL is identical to  $\mu$  at the center of the electrolyte where the electric potential  $\Psi = 0$ , yielding

$$\mu_s = \mu^o = \frac{k_B T}{\delta l^3} \ln \left( \frac{c_0}{1 - 2c_0} \right) \neq 0.$$

## 2. Young's law

In this part, we present our wetting boundary model is thermodynamically consistent with previous sharp interface models. we derive the Young's law. As the sessile droplet illustrated in figure 8, integrating  $\mu_s \delta l$  in the cylindrical coordinates from the equilibrium surface liquid composition  $c_0$  at the droplet center position  $r = 0$  to the equilibrium surface air composition  $c_\infty$  at  $r = \infty$ , yielding

$$\begin{aligned} \int_{c_0}^{c_\infty} \mu_s \delta l dc_s &= f_w(c_\infty) \delta l - f_w(c_0) \delta l - \int_{c_0}^{c_\infty} \left[ \kappa_s \frac{\partial c_s}{\partial r} \cos \theta + \frac{\kappa_s}{r} \frac{\partial}{\partial r} \left( r \frac{\partial c_s}{\partial r} \right) \delta l \right] dc_s \\ &= \gamma(c_\infty) - \gamma(c_0) - \sigma \cos \theta - \int_0^\infty \frac{\kappa_s}{r} \left( \frac{\partial c_s}{\partial r} \right)^2 \delta l dr \\ &= \Delta \gamma - \sigma \cos \theta - \frac{\tau_L \delta l}{r_c}, \end{aligned} \quad (\text{B5})$$

where the liquid-air interfacial tension reads  $\sigma := \int_0^\infty \kappa(\partial_r c_s)^2 dr$ , which is integrated along the droplet-air surface normal direction  $R$ ; see figure 8. Meanwhile, the solid-liquid and solid-air

interfacial tensions are represented by  $\gamma(c_0)$ ,  $\gamma(c_\infty)$ , respectively. Hence,  $\Delta\gamma = \gamma(c_\infty) - \gamma(c_0)$ . The contact line radius is  $r_c$ . More details on the parameter  $\tau_L := \int_0^\infty \kappa_s (\partial_r c_s)^2 dr$  is presented in our previous work [67].

Letting (B5) equal to 0, the Young's law with line tension effect [2, 34] is recovered,

$$\cos \theta = \frac{\Delta\gamma}{\sigma} - \frac{\tau_L \delta l}{\sigma r_c} + \mathcal{O}(r_c^{-2}). \quad (\text{B6})$$

Noteworthy, (B6) indicates the physical meaning of AL thickness  $\delta l$  from another perspective. In this work, we define the AL as the range of solid-fluid interactions from the energy perspective. Hence, at the distance farther than  $\delta l$  in the fluid bulk region, the fluid molecules are affected by the fluid-fluid interactions only, and no solid-fluid interaction exists. Consequently, AL and bulk fluid are intrinsically separated by the surface T locating at the position  $\delta l$  above the solid-fluid interface; see figure 7.

Based on this understanding, we suggest that the plane T is equivalent to the Gibbs dividing surface [20, 49]. Therefore,  $\delta l$  scales the magnitude of line tension effect which is in accordance with previous studies [56, 67].

- 
- [1] ALIPOUR, PEDRAM, TOGHRAIE, DAVOOD, KARIMIPOUR, ARASH & HAJIAN, MEHDI 2019 Molecular dynamics simulation of fluid flow passing through a nanochannel: effects of geometric shape of roughnesses. *Journal of Molecular Liquids* **275**, 192–203.
  - [2] AMIRFAZLI, A & NEUMANN, AW 2004 Status of the three-phase line tension: a review. *Advances in colloid and interface science* **110** (3), 121–141.
  - [3] BEDEAUX, DICK 1986 Nonequilibrium thermodynamics and statistical physics of surfaces. *Advances in chemical physics* **64**, 47–109.
  - [4] BOCQUET, LYDÉRIC & BARRAT, JEAN-LOUIS 1994 Hydrodynamic boundary conditions, correlation functions, and kubo relations for confined fluids. *Physical review E* **49** (4), 3079.
  - [5] BOTHE, DIETER 2022 Sharp-interface continuum thermodynamics of multicomponent fluid systems with interfacial mass. *International Journal of Engineering Science* **179**, 103731.
  - [6] BOTHE, DIETER & PRÜSS, JAN 2016 On the interface formation model for dynamic triple lines. In *Mathematical Fluid Dynamics, Present and Future: Tokyo, Japan, November 2014*, pp. 25–47. Springer.

- [7] BUI, ANNA T & COX, STEPHEN J 2024 Revisiting the green–kubo relation for friction in nanofluidics. *The Journal of Chemical Physics* **161** (20).
- [8] BUTT, HANS-JÜRGEN, BERGER, RÜDIGER, STEFFEN, WERNER, VOLLMER, DORIS & WEBER, STEFAN AL 2018 Adaptive wetting—adaptation in wetting. *Langmuir* **34** (38), 11292–11304.
- [9] CAHN, JOHN W & HILLIARD, JOHN E 1958 Free energy of a nonuniform system. i. interfacial free energy. *The Journal of chemical physics* **28** (2), 258–267.
- [10] CAI, YUHAN, WANG, FEI, ZHANG, HAODONG & NESTLER, BRITTA 2024 Chemo-elasto-electro free energy of non-uniform system in the diffuse interface context. *Journal of Physics: Condensed Matter* **36** (49), 495702.
- [11] CARLSON, ANDREAS, DO-QUANG, MINH & AMBERG, GUSTAV 2009 Modeling of dynamic wetting far from equilibrium. *Physics of fluids* **21** (12).
- [12] CHAN, TAK SHING, KAMAL, CATHERINE, SNOELJER, JACCO H, SPRITTLES, JAMES E & EGGERS, JENS 2020 Cox–voinov theory with slip. *Journal of fluid mechanics* **900**, A8.
- [13] CROSS, BENJAMIN, BARRAUD, CHLOÉ, PICARD, CYRIL, LÉGER, LILIANE, RESTAGNO, FRÉDÉRIC & CHARLAIX, ÉLISABETH 2018 Wall slip of complex fluids: Interfacial friction versus slip length. *Physical Review Fluids* **3** (6), 062001.
- [14] CUI, GUANDONG, XU, ZHI, LI, HAN, ZHANG, SHUCHEN, XU, LUPING, SIRIA, ALESSANDRO & MA, MING 2023 Enhanced osmotic transport in individual double-walled carbon nanotube. *Nature Communications* **14** (1), 2295.
- [15] DE GENNES, PIERRE GILLES 1981 Polymer solutions near an interface. adsorption and depletion layers. *Macromolecules* **14** (6), 1637–1644.
- [16] DE GENNES, PIERRE-GILLES 1985 Wetting: statics and dynamics. *Reviews of modern physics* **57** (3), 827.
- [17] DING, GUANG-YU & XIA, KE-QING 2023 Heat transport and flow morphology of geostrophic rotating rayleigh–bénard convection in the presence of boundary flow. *Journal of Fluid Mechanics* **975**, A46.
- [18] DING, HANG & SPELT, PETER DM 2007 Wetting condition in diffuse interface simulations of contact line motion. *Physical Review E—Statistical, Nonlinear, and Soft Matter Physics* **75** (4), 046708.
- [19] DONG, W 2021 Thermodynamics of interfaces extended to nanoscales by introducing integral

- and differential surface tensions. *Proceedings of the National Academy of Sciences* **118** (3), e2019873118.
- [20] GIBBS, JOSIAH WILLARD 1928 *The Collected Works of J. Willard Gibbs...: Thermodynamics*, vol. 1. Longmans, Green and Company.
- [21] HADJICONSTANTINO, NG 2021 An atomistic model for the navier slip condition. *Journal of Fluid Mechanics* **912**, A26.
- [22] HADJICONSTANTINO, NICOLAS G 2024 Molecular mechanics of liquid and gas slip flow. *Annual Review of Fluid Mechanics* **56** (1), 435–461.
- [23] HOCKING, LM 1977 A moving fluid interface. part 2. the removal of the force singularity by a slip flow. *Journal of Fluid Mechanics* **79** (2), 209–229.
- [24] HOLEY, HANNES, GUMBSCH, PETER & PASTEWKA, LARS 2023 Confinement-induced diffusive sound transport in nanoscale fluidic channels. *Physical review letters* **131** (8), 084001.
- [25] HUH, CHUN & SCRIVEN, LAURENCE E 1971 Hydrodynamic model of steady movement of a solid/liquid/fluid contact line. *Journal of colloid and interface science* **35** (1), 85–101.
- [26] JACQMIN, DAVID 2000 Contact-line dynamics of a diffuse fluid interface. *Journal of fluid mechanics* **402**, 57–88.
- [27] JOSEPH, PIERRE & TABELING, PATRICK 2005 Direct measurement of the apparent slip length. *Physical Review E—Statistical, Nonlinear, and Soft Matter Physics* **71** (3), 035303.
- [28] KANNAM, SRIDHAR KUMAR, TODD, BD, HANSEN, JESPER SCHMIDT & DAIVIS, PETER J 2013 How fast does water flow in carbon nanotubes? *The Journal of chemical physics* **138** (9).
- [29] KANSAL, MINKUSH, DATT, CHARU, BERTIN, VINCENT & SNOEIJER, JACCO H 2025 Viscoelastic wetting transition: beyond lubrication theory. *The European Physical Journal Special Topics* pp. 1–19.
- [30] KUMAR KANNAM, SRIDHAR, TODD, BD, HANSEN, JESPER SCHMIDT & DAIVIS, PETER J 2012 Slip length of water on graphene: Limitations of non-equilibrium molecular dynamics simulations. *The Journal of chemical physics* **136** (2).
- [31] KUSUMAATMAJA, HALIM, HEMINGWAY, EWAN J & FIELDING, SUZANNE M 2016 Moving contact line dynamics: from diffuse to sharp interfaces. *Journal of Fluid Mechanics* **788**, 209–227.
- [32] LAUGA, ERIC, BRENNER, MICHAEL P & STONE, HOWARD A 2005 Microfluidics: the no-slip boundary condition. *arXiv preprint cond-mat/0501557* .

- [33] LAUGA, ERIC & STONE, HOWARD A 2003 Effective slip in pressure-driven stokes flow. *Journal of Fluid Mechanics* **489**, 55–77.
- [34] LAW, BRUCE M, MCBRIDE, SEAN P, WANG, JIANG YONG, WI, HAENG SUB, PANERU, GOVIND, BETELU, SANTIGO, USHIJIMA, BAKU, TAKATA, YOUICHI, FLANDERS, BRET, BRESME, FERNANDO & OTHERS 2017 Line tension and its influence on droplets and particles at surfaces. *Progress in surface science* **92** (1), 1–39.
- [35] LUCHINI, PAOLO 2013 Linearized no-slip boundary conditions at a rough surface. *Journal of fluid mechanics* **737**, 349–367.
- [36] MAALI, ABDELHAMID & BHUSHAN, BHARAT 2012 Measurement of slip length on superhydrophobic surfaces. *Philosophical Transactions of the Royal Society A: Mathematical, Physical and Engineering Sciences* **370** (1967), 2304–2320.
- [37] MAXWELL, JAMES CLERK 1879 Vii. on stresses in rarified gases arising from inequalities of temperature. *Philosophical Transactions of the royal society of London* (170), 231–256.
- [38] MOFFATT, H KEITH 1964 Viscous and resistive eddies near a sharp corner. *Journal of Fluid Mechanics* **18** (1), 1–18.
- [39] MURALIDHAR, PRANESH, FERRER, NANGELIE, DANIELLO, ROBERT & ROTHSTEIN, JONATHAN P 2011 Influence of slip on the flow past superhydrophobic circular cylinders. *Journal of Fluid Mechanics* **680**, 459–476.
- [40] MYERS, TIM G 2011 Why are slip lengths so large in carbon nanotubes? *Microfluidics and nanofluidics* **10**, 1141–1145.
- [41] NAVIER, CLAUDE 1822 *Mémoire sur les lois du mouvement des fluides*. éditeur inconnu.
- [42] NETO, CHIARA, EVANS, DREW R, BONACCURSO, ELMAR, BUTT, HANS-JÜRGEN & CRAIG, VINCENT SJ 2005 Boundary slip in newtonian liquids: a review of experimental studies. *Reports on progress in physics* **68** (12), 2859.
- [43] QIAN, TIEZHENG, QIU, CHUNYIN & SHENG, PING 2008 A scaling approach to the derivation of hydrodynamic boundary conditions. *Journal of Fluid Mechanics* **611**, 333–364.
- [44] QIAN, TIEZHENG, WANG, XIAO-PING & SHENG, PING 2003 Molecular scale contact line hydrodynamics of immiscible flows. *Physical Review E* **68** (1), 016306.
- [45] QIAN, TIEZHENG, WANG, XIAO-PING & SHENG, PING 2004 Power-law slip profile of the moving contact line in two-phase immiscible flows. *Physical review letters* **93** (9), 094501.
- [46] QIAN, TIEZHENG, WANG, XIAO-PING & SHENG, PING 2006 A variational approach to mov-

- ing contact line hydrodynamics. *Journal of Fluid Mechanics* **564**, 333–360.
- [47] RAMOS-ALVARADO, BLADIMIR, KUMAR, SATISH & PETERSON, GP 2016 Hydrodynamic slip length as a surface property. *Physical Review E* **93** (2), 023101.
- [48] REN, WEIQING, TRINH, PHILIPPE H & WEINAN, E 2015 On the distinguished limits of the navier slip model of the moving contact line problem. *Journal of Fluid Mechanics* **772**, 107–126.
- [49] SCHIMMELE, L, NAPIÓRKOWSKI, M & DIETRICH, S 2007 Conceptual aspects of line tensions. *The Journal of chemical physics* **127** (16).
- [50] SECCHI, ELEONORA, MARBACH, SOPHIE, NIGUÈS, ANTOINE, STEIN, DEREK, SIRIA, ALESSANDRO & BOCQUET, LYDÉRIC 2016 Massive radius-dependent flow slippage in carbon nanotubes. *Nature* **537** (7619), 210–213.
- [51] SHIKHMURZAEV, YULII D 1993 The moving contact line on a smooth solid surface. *International Journal of Multiphase Flow* **19** (4), 589–610.
- [52] SNOEIJER, JACCO H 2006 Free-surface flows with large slopes: Beyond lubrication theory. *Physics of Fluids* **18** (2).
- [53] THOMAS, JOHN A & MCGAUGHEY, ALAN JH 2008 Reassessing fast water transport through carbon nanotubes. *Nano letters* **8** (9), 2788–2793.
- [54] VORONOV, ROMAN S, PAPAVALASSIOU, DIMITRIOS V & LEE, LLOYD L 2006 Boundary slip and wetting properties of interfaces: Correlation of the contact angle with the slip length. *The Journal of chemical physics* **124** (20).
- [55] WANG, FEI & NESTLER, BRITTA 2024 Wetting and contact-angle hysteresis: Density asymmetry and van der waals force. *Physical Review Letters* **132** (12), 126202.
- [56] WANG, FEI, ZHANG, HAODONG & NESTLER, BRITTA 2024 Wetting phenomena: Line tension and gravitational effect. *Physical Review Letters* **133** (24), 246201.
- [57] WANG, FEI, ZHANG, HAODONG, WU, YANCHEN & NESTLER, BRITTA 2023 A thermodynamically consistent diffuse interface model for the wetting phenomenon of miscible and immiscible ternary fluids. *Journal of Fluid Mechanics* **970**, A17.
- [58] WANG, XIAO-PING, QIAN, TIEZHENG & SHENG, PING 2008 Moving contact line on chemically patterned surfaces. *Journal of fluid mechanics* **605**, 59–78.
- [59] WEN, BAOLE, GOLUSKIN, DAVID & DOERING, CHARLES R 2022 Steady rayleigh–bénard convection between no-slip boundaries. *Journal of Fluid Mechanics* **933**, R4.

- [60] XIA, KE-QING 2024 Unveiling the mystery of effective slip. *Journal of Fluid Mechanics* **1000**, F5.
- [61] XIE, QUAN, ALIBAKHSHI, MOHAMMAD AMIN, JIAO, SHUPING, XU, ZHIPING, HEMPEL, MAREK, KONG, JING, PARK, HYUNG GYU & DUAN, CHUANHUA 2018 Fast water transport in graphene nanofluidic channels. *Nature nanotechnology* **13** (3), 238–245.
- [62] YARIV, E 2023 Effective slip length for transverse shear flow over partially invaded grooves. *Journal of Fluid Mechanics* **957**, R1.
- [63] YUE, PENGTAO 2020 Thermodynamically consistent phase-field modelling of contact angle hysteresis. *Journal of Fluid Mechanics* **899**, A15.
- [64] YUE, PENGTAO & FENG, JAMES J 2012 Phase-field simulations of dynamic wetting of viscoelastic fluids. *Journal of Non-Newtonian Fluid Mechanics* **189**, 8–13.
- [65] YUE, PENGTAO, ZHOU, CHUNFENG & FENG, JAMES J 2010 Sharp-interface limit of the cahn–hilliard model for moving contact lines. *Journal of Fluid Mechanics* **645**, 279–294.
- [66] ZHANG, HAODONG, WANG, FEI & NESTLER, BRITTA 2022 Janus droplet formation via thermally induced phase separation: a numerical model with diffusion and convection. *Langmuir* **38** (22), 6882–6895.
- [67] ZHANG, HAODONG, WANG, FEI & NESTLER, BRITTA 2023 Line tension of sessile droplets: Thermodynamic considerations. *Physical Review E* **108** (5), 054121.
- [68] ZHANG, HAODONG, WANG, FEI & NESTLER, BRITTA 2024 Multi-component electro-hydro-thermodynamic model with phase-field method. i. dielectric. *Journal of Computational Physics* p. 112907.
- [69] ZHANG, HAODONG, WU, YANCHEN, WANG, FEI, GUO, FUHAO & NESTLER, BRITTA 2021 Phase-field modeling of multiple emulsions via spinodal decomposition. *Langmuir* **37** (17), 5275–5281.
- [70] ZHANG, HAODONG, ZHANG, HONGMIN, WANG, FEI & NESTLER, BRITTA 2024 Wetting effect induced depletion and adsorption layers: Diffuse interface perspective. *ChemPhysChem* p. e202400086.